Enhancement of Piezoelectricity in Dimensionally Engineered Metal-Halide Perovskites Induced by Deep Level Defects

Sung Heo, Do Yoon Lee, Dongwook Lee, Yonghui Lee, Kihong Kim, Hyun-Sung Yun, Min Jae Paik, Tae Joo Shin, Hyeon Seung Oh, Taeho Shin, Jaekyung Kim, Seong Heon Kim,* Sang Il Seok,* and Mohammad Khaja Nazeeruddin*

Metal halide perovskite solar cells (PSCs) have been considered to be one of the most promising next-generation energy harvesters over the past decades due to remarkably rapid improvement of power conversion efficiency in photovoltaics. However, energy harvesters based on the solar energy source have an intrinsic environment limitation for indoor applications. A feasible solution to the limitation is to add non-solar energy harvesting functions to the solar energy harvesters. Here, the piezoelectric properties of two types of metal halide PSCs are investigated, the 3D only and the 3D/2D structure, showing PCEs of 21.3% and 23.2%, respectively. Piezo-response force microscopy and synchrotron-based X-ray diffraction demonstrate that both types of PSC sample have piezoelectricity. Remarkably, the 3D/2D structure has considerably higher piezoelectric amplitude than the 3D-only. The deep level transient spectroscopy results reveal that the enhancement in the piezoelectricity of the 3D/2D structure originates from Pb_{Br} defects. This study unravels the role of defects in the piezoelectricity of metal halide PSCs and provides a direction to develop the multi-function energy harvesters based on the PSCs.

1. Introduction

Global warming/climate change and environmental pollution caused by primary fossil fuel consumption have been discussed as a vital issue of our time worldwide. Renewable energies as alternative energy sources to traditional fossil fuels have been exploited due to their eco-friendliness and sustainability. Among the sustainable energy such as heat and wind, sunlight is the most feasible and available in the ambient environment. Over the past few decades, extensive research has been devoted to elevating the power conversion efficiency (PCE) of solar cells, resulting in the commercialization of Si solar cells,[1–5] cadmium telluride (CdTe),[6–9] and copper indium gallium selenide (CIGS).[10,11] However, the cost and the complex fabrication processes of these technologies are still the biggest obstacles to the widespread

S. Heo, K. Kim
Samsung Advanced Institute of Technology
130, Samsung-ro, Yeongtong-gu, Suwon 16678, Korea
D. Y. Lee, Y. Lee, H.-S. Yun, M. J. Paik, S. I. Seok
School of Energy and Chemical Engineering
Ulsan National Institute of Science and Technology
50 UNIST-gil, Eonyang-eup, Ulju-gun, Ulsan 44919, Republic of Korea
E-mail: seoksi@unist.ac.kr
D. Lee
Department of Physics
College of Science and Technology
1 Yonseidae-gil, Wonju, Gangwon-do, Ulsan 26493, Republic of Korea

The ORCID identification number(s) for the author(s) of this article can be found under https://doi.org/10.1002/aenm.202200181.

T. J. Shin
Graduate School of Semiconductor Materials and Devices Engineering
Ulsan National Institute of Science and Technology
50 UNIST-Gil, Eonyang-eup, Ulju-gun, Ulsan 44919, Republic of Korea
H. S. Oh, T. Shin
Department of Chemistry
Jeonbuk National University
Jeonju 54896, Republic of Korea
J. Kim
Research Application Technology Center
Park Systems, 109 Gwanggyo-ro, Suwon 16229, Republic of Korea
S. H. Kim
Department of Physics
Research Institute of Physics and Chemistry
Jeonbuk National University
Jeonju 54896, Republic of Korea
E-mail: shkim97@jbnu.ac.kr
M. K. Nazeeruddin
Group for Molecular Engineering of Functional Materials
Ecole Polytechnique Fédérale de Lausanne
Sion CH-1951, Switzerland
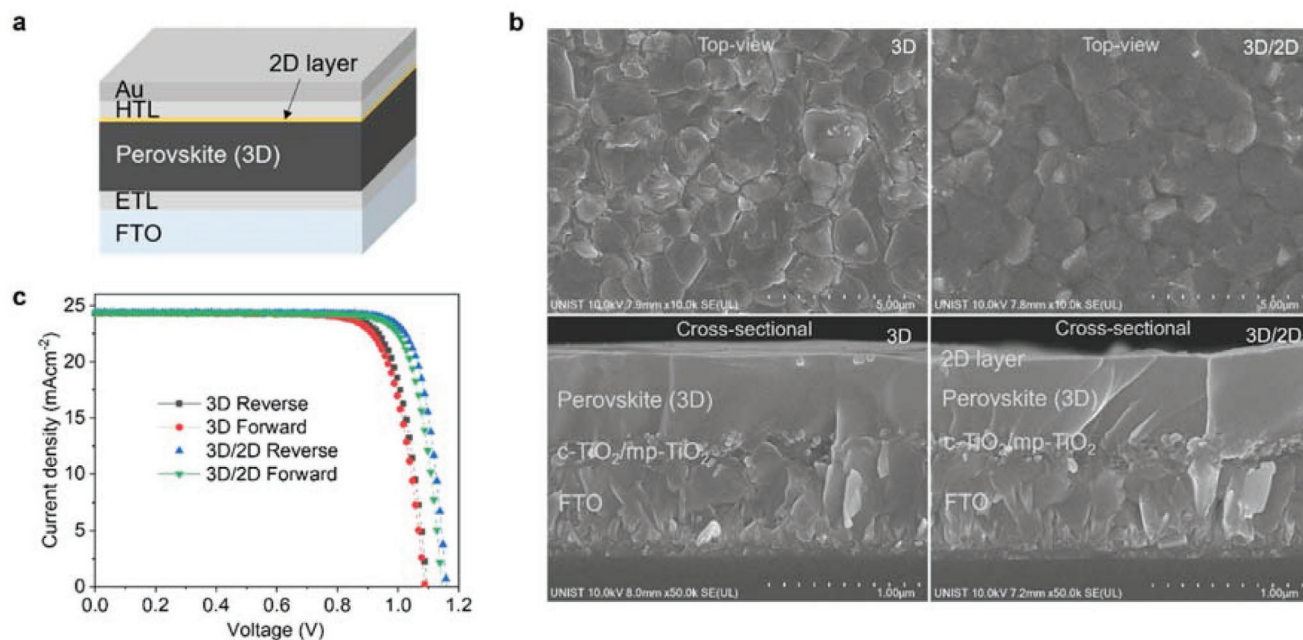E-mail: mdkhaja.nazeeruddin@epfl.ch

Figure 1. Perovskite solar cells with and without the 2D interlayer. a) Device structure. b) SEM top-view (top) and cross-sectional (bottom) images. c) J–V curves change with and without the 2D layer.

commercialization of solar cells. The strong demands for solar cells with simple and low-cost fabrication processes have led to the invention of organic metal halide perovskite solar cells (PSCs), which are prepared by simple and inexpensive solution-processed fabrication.[12–14] The metal halide PSCs pioneered by Kojima et al.[15] have achieved remarkable improvement in the PCE from 3.8%[15] to 25.7%[16] and have been anticipated to surpass the conventional solar cells once some critical issues such as stability and scale-up are dealt with. Despite the splendid performance of PSCs, they have the environmental limit as indoor electronic devices because they require daylight, i.e., sunlight. Thus, the limit would be removed if the electricity is to be acquired from two energy sources. In the meantime, there have been efforts to integrate multi-source energy harvesters on a single device,[17–19] but most of them were only serial connections of energy harvesters. Therefore, it is crucial for the commercialization to develop energy harvesters that possess multiple energy harvesting functions in a straightforward structure.[20]

Piezoelectricity allows obtaining clean and sustainable energy through the conversion of mechanical energy into electrical energy. Many energy harvesters based on piezoelectricity have been developed over the last decade.[21–24] Recently, the piezoelectric PSCs have attracted research attention because the perovskite materials are reported to hold piezoelectric and ferroelectric properties,[25–33] making it highly feasible to realize the PSCs with dual-energy harvesting functions by obtaining electricity from the solar/mechanical energy simultaneously without changing the original PSC structure optimized for the high PCE. Here, we report that deep-level defects play a crucial role in enhancing piezoelectric properties for the 3D/2D samples. The piezo-response force microscopy (PFM) and the synchrotron-based X-ray diffraction (XRD) measurements reveal that both types of samples have piezoelectric properties

and the 3D/2D sample has considerably higher piezoelectric intensity than the 3D-only. Deep level transient spectroscopy (DLTS) results unveil that the anomalous piezoelectric effect in the 3D/2D sample is due to the Pb_{Br} defects.

2. Results and Discussion

Figure 1a shows a device structure investigated in this work, which consists of fluorine-doped SnO_2 (FTO)/compact-TiO_2 (c-TiO_2)/mesoporous-TiO_2(mp-TiO_2)/3D(/2D)/spiro-OMeTAD/gold layers.[34,35] It appears that the 2D layer uniformly covers the 3D layer on the scanning electron microscopy (SEM) top-view images without visible change of thickness according to the SEM cross-sectional images shown in Figure 1b. Although a thin 2D layer is formed on top of the 3D layer, the influence of the 2D interlayer on the device performance seems quite huge, as seen in the J–V curve measurement (Figure 1c). The devices without and with the 2D layer show the PCE of 21.3% and 23.2%, respectively, due to an increase of open-circuit voltage (V_{oc}) and fill factor (FF). Small J–V curve hysteresis is still observed from both cells.

Considering that the 2D layer has a certain thickness, the 3D/2D structure can cause a decrease in the relative dielectric constant of the entire perovskite film due to the serial connection, resulting in a change of dielectric properties related to an electrical polarization. To verify the dielectric change, the film surfaces were characterized by PF Min vertical mode. The schematic of the setup is depicted in **Figure 2**a. Typically, two types of data, amplitude and phase, are acquired with PFM They indicate the piezoelectric intensity and the polarization direction, respectively. Figure 2b,c illustrates the piezo-response curves of the 3D-only and the 3D/2D samples. The curves specify that both types of PSC samples have piezoelectricity. In comparing
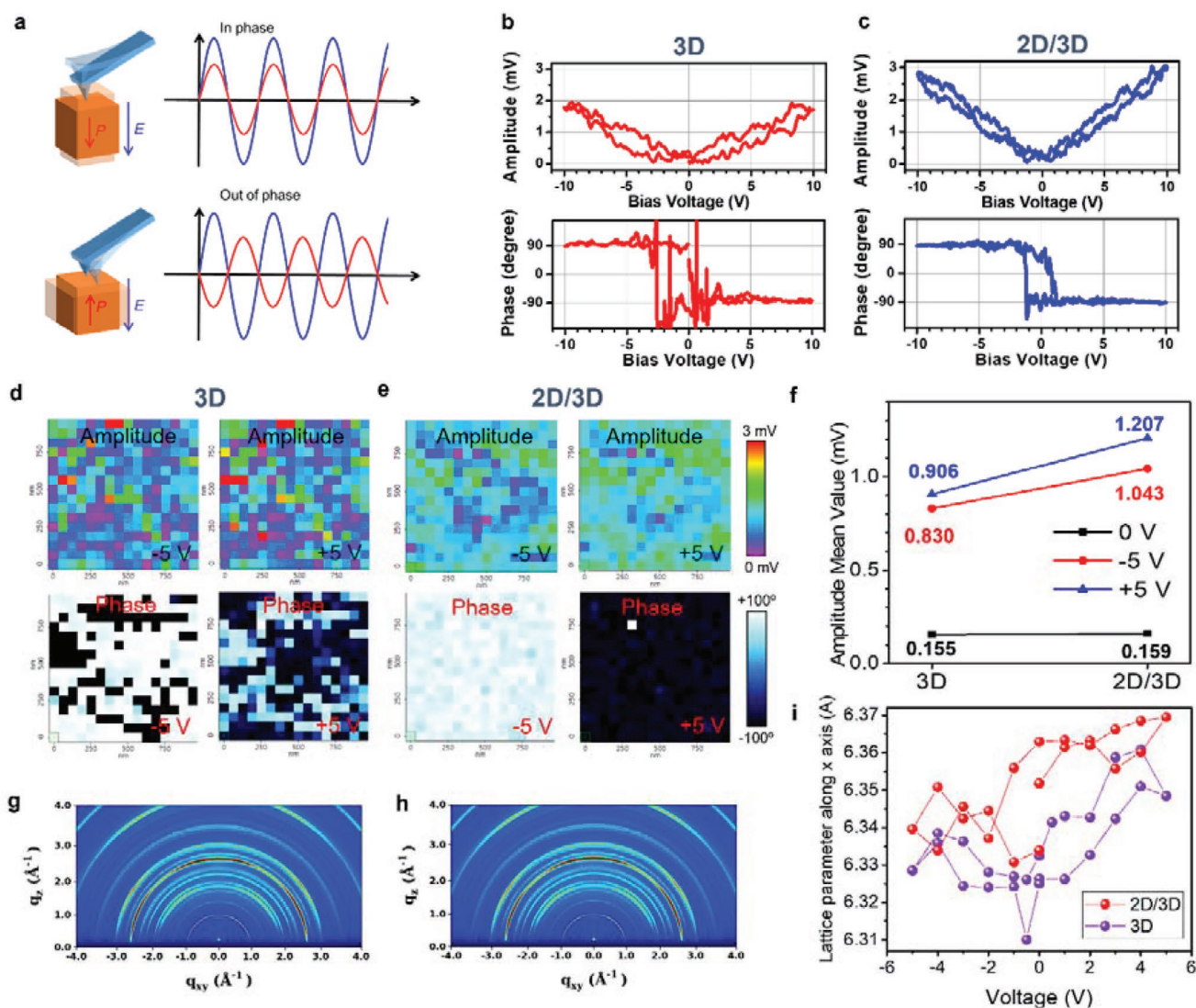
Figure 2. Piezoelectric property of the perovskite device. a) Schematic of vertical PFM mode: in-phase and out-of-phase. b) Piezoresponses curves of the 3D-only. c) Piezoresponses curves of the 3D/2D sample. d) Amplitude and phase maps of the 3D-only. e) Amplitude and phase maps of the 3D/2D sample. f) Mean values of piezoelectric amplitude averaged over the maps in Figure 2d,e. g) GIXD patterns of the perovskite layers the 3D-only. h) GIXD patterns of the perovskite layers 3D/2D. i) Lattice parameters along the (001) direction vs bias voltages.

the piezoelectric intensities (amplitude values) in Figure 2b,c, the 3D/2D sample remarkably shows ≈1.5 times higher amplitude than that of the 3D-only one, i.e., the piezoelectric intensity of the 3D/2D sample increases more than the 3D-only device despite the serially connected capacitor structure. To corroborate this finding, the 2D maps were made by measuring 256 piezoelectric curves (16 pixels × 16 pixels) on an area of 1 μm × 1 μm. Figure 2d,e displays the amplitude and phase maps biased at voltages of +5 and −5 V. The amplitude maps at ±5 V for both the 3D-only and the 3D/2D samples show almost homogeneous contrast within the acquisition areas of 1 μm × 1 μm, and the 3D/2D sample has a higher intensity than the 3D-only. The mean values of piezoelectric amplitude, averaged over the amplitude maps in Figure 2c, are plotted in Figure 2f. The amplitude mean values for the 3D/2D sample (1.207 mV at +5 V and 1.043 mV at −5 V) are approximately

higher than those for the 3D-only sample (0.906 mV at +5 V, 0.830 mV at −5 V). This coincides with the result discussed in Figure 2b,c, confirming that the 3D/2D structure has stronger piezoelectric properties than the 3D-only device. Grazing incidence X-ray diffraction (GIXD) patterns of the perovskite samples in Figure 2g,h display Debye–Scherrer diffraction rings, indicating that both samples have polycrystalline phases with randomly oriented grains. The GIXD patterns of the samples were also acquired by applying bias voltages between the top electrode and the bottom electrode of the samples. The lattice parameters of the samples along the (001) direction are illustrated in Figure 2i. The lattice parameters vary with the applied bias voltage. This phenomenon, the dependence of the lattice parameter on the external electrical field, is called an inverse piezoelectric effect. The inverse piezoelectric effect appears in both samples, but the percentage of the change in the lattice
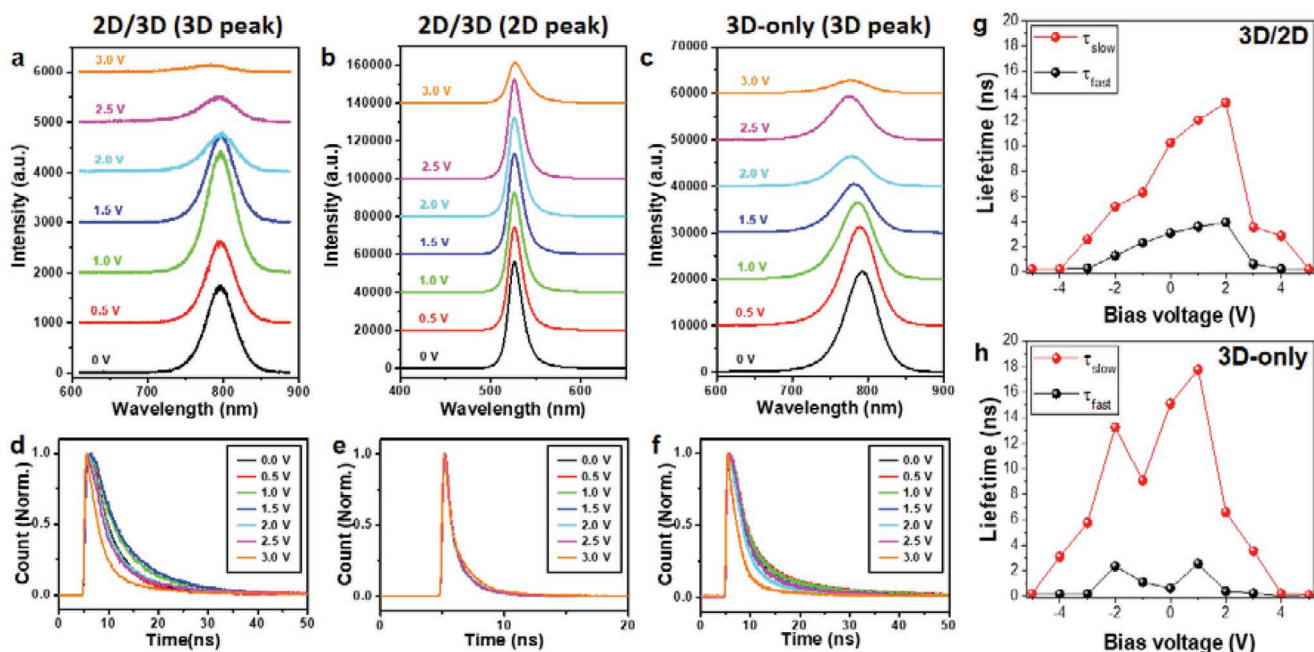
**ADVANCED
SCIENCE NEWS**
www.advancedsciencenews.com

**ADVANCED
ENERGY
MATERIALS**
www.advenergymat.de

Figure 3. Photoluminescence characteristics under bias. a,b) Emission characteristics of the 3D/2D perovskite layer under applied bias voltages. c) Emission characteristics of the 3D-only perovskite layer under applied bias voltages. d,e) Decay curves of the 3D and 2D region emissions of the 3D/2D layer with the applied bias voltages. f) Decay curves of the 3D-only with the applied bias voltages. g,h) Decay curves of 3D/2D and 3D-only perovskite films fitted using a bi-exponential function and the lifetimes.

parameter is higher in the 3D/2D than the 3D-only; in other words, the intensity of the piezoelectricity in the 3D/2D is stronger than that in the 3D-only.

To elucidate the origin of the piezoelectric properties of the 3D and 3D/2D PSCs, the transient photoluminescence (P.L.) spectroscopy measurements were carried out with the applied bias voltage. **Figure 3**a,b illustrates the emission characteristics of the 3D/2D. The excitation wavelength was 488 nm, and the emission lines were collected with the bias voltage. The luminescence at 796 nm of the 3D/2D shows a blue shift, and the intensity diminishes as the bias voltage increases (Table S1, Supporting Information), while the peak at 527 nm shrinks without a shift in the peak position (Table S2, Supporting Information). As for the 3D-only (Figure 3c), the peak at 790 nm shows a blue shift and the intensity decreases as the bias voltage increases (Table S3, Supporting Information). The electric field between the electrodes causes the structural change of the PSCs, leading to the change of band structure. As a result, the PL intensity decreases as the bias voltage increases. In the 3D layers in both samples, the PL intensity decreases dramatically with the bias voltage, while that on the 2D layer gradually becomes smaller with the bias voltage. This reveals that the bandgaps of the 3D layers in both samples are more influenced by the external field than that of the 2D layer. There is also a remarkable difference between the decay curves of the 3D/2D and the 3D-only in Figure 3d–f. The PL intensity at 797 nm of the 3D/2D in Figure 3d decays obviously slower as the bias voltage increases from 0V to 1.5 V, while the decay becomes faster above 1.5 V. Generally, the charge recombination at defects leads to a short lifetime, i.e., the defect density of the 3D/2D initially decreases with the bias voltage while it increases again above

1.5 V. The decay curves of the 3D/2D at 527 nm in Figure 3e seem to be independent of the bias voltage, while the PL curves of the 3D-only at 797 nm in Figure 3f becomes faster as the bias voltage increases. The anomalous PL decay of the 3D/2D at 797 nm in Figure 3d is likely to be caused by the migration of iodine atoms from the 2D side to the 3D side because the 3D/2D sample might have a relatively higher ratio of I/Br than the 3D-only. I-rich perovskites have a longer PL lifetime than Br-rich perovskite.[36–39] The decay curves were also fitted using a bi-exponential function, and the lifetimes (τ_{fast}, τ_{slow}) are displayed in Figure 3g,h. The lifetimes (τ_{fast} and τ_{slow}) of the 3D/2D show asymmetric behavior with the bias voltage, while they seem to be rather symmetric in the 3D-only. The lifetimes of the fast decay (τ_{fast}) in the 3D-only are shorter than those of the 3D/2D, indicating that there are more trap sites such as shallow level states which lead to the fast relaxation.

Deep-level defects have a strong influence on the performances of devices, including solar cells.[36–40] DLTS measurements were carried out to unveil the role of defects in piezoelectricity. **Figure 4** exhibits the DLTS results for the samples. In Figure 4a, two peaks are distinct at 370 K (E1) and 440 K (E3). As the bias voltage increases from the negative to the positive, the 400 K (E2) peak grows much bigger than the 370 K (E1) peak and becomes dominant. In our previous study, the E1, E2, and E3 were ascribed to I_{Pb}, I_{Ma}, and Pb_{Br}, respectively.[39–41] The DLTS spectra of the 3D/2D display three peaks at 370 K, 400 K, and 440 K. As the bias voltage increases from the negative to the positive, the peaks of E2 and E3 grow bigger, and only the peak of E1 becomes negligible. The deep level defects in the 3D-only and the 3D/2D show different trends, i.e., the E2 becomes dominant in the 3D-only, while the E3 is prevailing
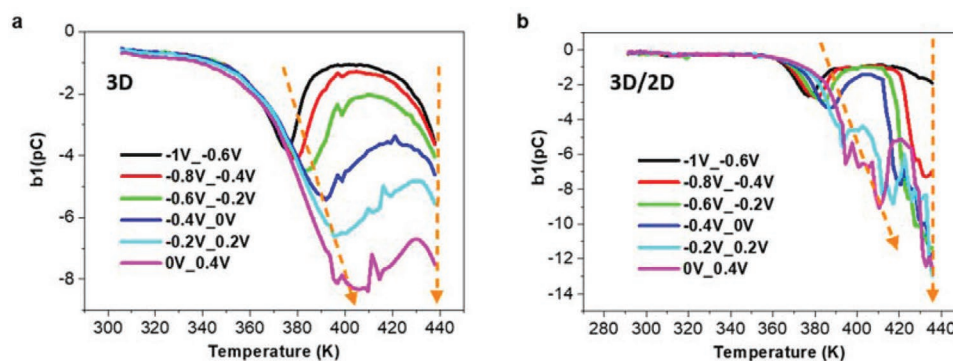
ADVANCED
SCIENCE NEWS
www.advancedsciencenews.com

ADVANCED
ENERGY
MATERIALS
www.advenergymat.de

Figure 4. Deep level traps in the perovskite films. a) DLTS spectra of the 3D film with the applied bias voltages. b) DLTS spectra of the 3D/2D film with the applied bias voltages.

in the 3D/2D. The peak intensities of the E2 and E3 in the 3D/2D are much higher than those of the 3D-only, implying that the 3D/2D is rich in E2 and E3 defects. Although the two peaks increase as the bias voltage increases in the 3D-only, the peak from E3 in the 3D/2D rapidly grows further as the bias increases from −1 V to 0.4 V. Since the 2D layer is on the 3D layer in the sample, the E3 defects in the 2D layer are more susceptible to the increase of the bias voltage. Figure 4a,b reveals that E1 and E3 defects are abundant in the 3D layer, while 2D has many E3 defects. In connecting the DLTS results with the piezo-responses in Figure 2, the increase of the peak is associated with the piezo-responses (See **Table 1**). Compared with the 3D-only, the 3D/2D has a higher density of the E3 defect. Because the E3 (Pb_Br) defects are so electrically positive, they are more likely to be strongly polarized. As the density of the E3 increases, the contribution to the polarization by the defects becomes dominant, leading to the enhancement of the piezo-responses because charged defects often boost the dielectric polarization in various materials.[42–44]

3. Conclusion

Scheme 1 illustrates the electrical polarization in the samples. The 3D-only has no built-up charges without external stress (or pressure), although there is dielectric polarization caused by

electronic, ionic, dipolar, and space-charge polarization, which are ignored in Scheme 1. Upon the stress, the spontaneously polarized charges appear at the surfaces, resultantly increasing the polarization. E2 and E3 defects inside the 3D-only increase the polarization. However, their contribution to the polarization depends on the alignments of the charges inside the defects. Without proper alignment, most of the locally induced polarization by the defects would be canceled out or cause a slight change in piezoelectricity because the E2 and E3 defects have different signs. According to the previous study,[40] the 3D/2D sample has a 2D hole gas (2-DHG, positive 2D electron gas (2-DEG)) structure at the interface without external stress, in other words, quantum well structure for holes is formed in the 3D/2D perovskite heterojunction, and holes are more likely to stay at the interface.

Consequently, more positive and negative charges stay near the 2D and the 3D interface. Upon stress, extra charges are built up, and the 2-DHG enhances the polarization. Additionally, the intensity of the polarization increases in the 2D region due to the deep level defects, especially E3 defects, which are electrically positive and rich in the 2D region, while the negative polarization increases in the 3D region owing to the E2 defects. Instead of developing long-range polarization between the E2 and E3 defects, they develop local polarization in each region, like dopants or vacancies in oxides.[45–48] As a result, the 2-DHG and the alignment of the deep-level defects in the

Table 1. Defect parameters: activation energy, defect density, and cross section calculated from the DLTS spectra.

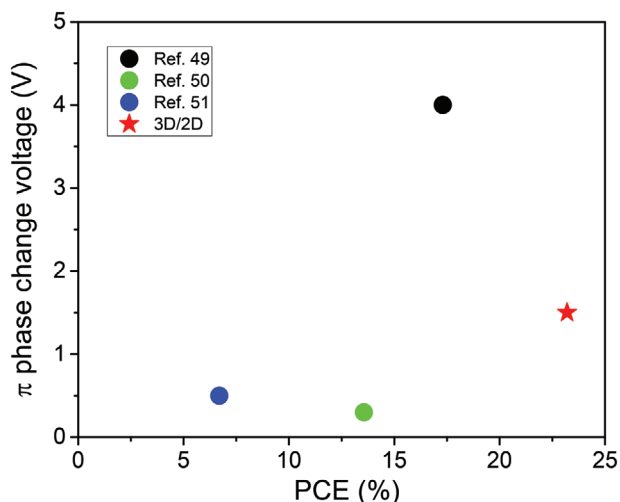| Parameters		3D			3D/2D		
		E1	E2	E3	E1	E2	E3
Forward region	Et [eV]		0.76	0.83	0.65	0.75	0.81
	Nt [cm^{-3}]		5.2×10^{15}	6.2×10^{15}	1.2×10^{15}	3×10^{15}	8.5×10^{15}
	Cross-section [σ, cm^2]		1.1×10^{-15}	0.5×10^{-15}	2×10^{-15}	1×10^{-15}	6×10^{-16}
Reverse region	Et [eV]	0.66	0.76	0.83	0.65	0.75	0.83
	Nt [cm^{-3}]	3.1×10^{16}	5.2×10^{16}	1.2×10^{16}	1.0×10^{16}	8.5×10^{15}	3.2×10^{15}
	Cross section [σ, cm^2]	4.1×10^{-15}	1.1×10^{-15}	0.5×10^{-15}	2×10^{-15}	1×10^{-15}	6×10^{-16}
Carrier concentration			9.1×10^{17}			1.3×10^{18}	
I/Pb (=E1 defect)			I/C (=E2 defect)			Pb/Br (=E3 defect)	
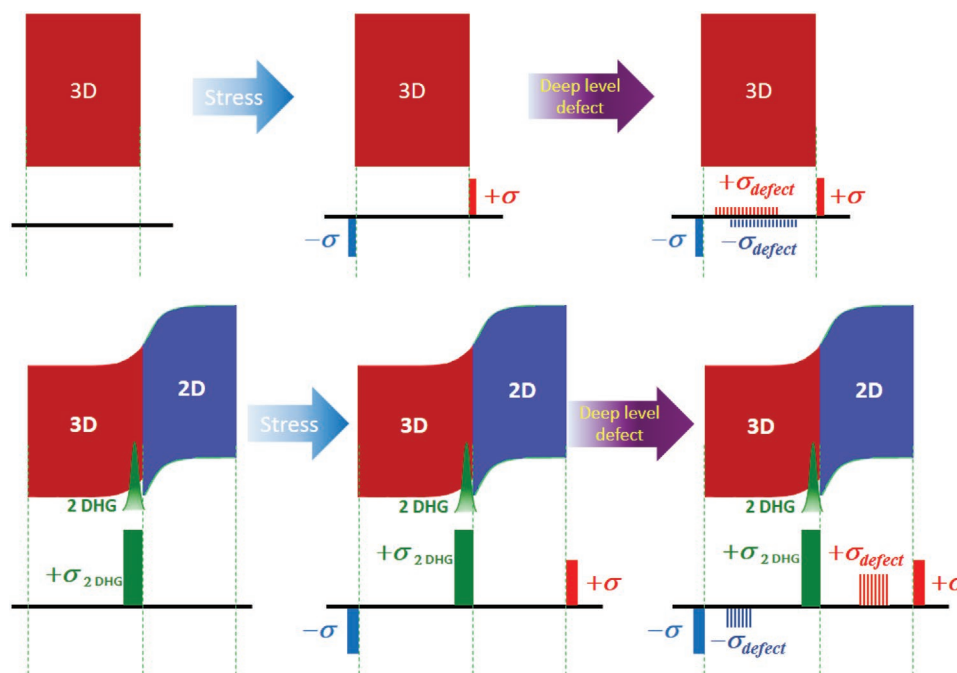
Scheme 1. Schematic band diagram for the 3D-only and the 3D/2D and the induced charges under stress due to the 2-DHG and the deep level defects.

3D/2D cooperate to yield strong piezoelectricity. Resultantly, the 2-DHG structure and deep-level defects work out together to yield the piezoelectricity with the help of electron blocking stability. Nevertheless, they are not the main components in the piezoelectricity that fundamentally relies on the electrical polarization of materials, although the 3D/2D structure is best for energy harvest and multi-functional energy collection.

Scheme 2 illustrates the solar cell PCE and π phase change voltage of different multi-functional devices. The 3D/2D dealt with in this work displays improved solar cell PCE and π phase change voltage compared to other multi-functional devices.[49–51] The 3D/2D shows excellent performance properties, unlike the other devices exhibiting only one auspicious characteristic: PCE or π phase change voltage. In this study, we investigated the piezoelectricity of two types of FAPbI$_3$-MAPbBr$_3$ PSC samples, the 3D-only and the 3D/2D structure, with the outstanding PCE performance of 21.3% and 23.2%, respectively. The results of the PFM and the synchrotron-based XRD measurements demonstrate that the two types of samples hold piezoelectric properties, and the 3D/2D has much stronger piezoelectric properties than the 3D-only. Moreover, the DLTS measurements indicate that the Pb$_{Br}$ defects play a crucial role in improving piezoelectric properties for the PSCs of the 3D/2D heterostructure.

4. Experimental Section

Device Fabrication: A dense blocking layer of TiO$_2$ ($\approx$30 nm in thickness, bl-TiO$_2$) was deposited onto an FTO substrate by spray pyrolysis using titanium diisopropoxidebis(acetylacetonate) in ethanol (1/10, v/v) at 450 °C. A 150-nm-thick layer of mesoporous TiO$_2$ was spin-coated at 1500 rpm onto the FTO/c-TiO$_2$ substrate using a TiO$_2$ paste diluted with 2-methoxyethanol, and then annealed at 500 °C for 1 h to remove the organic components.

A 1.26 M precursor of NH$_2$CH=NH$_2$(= F.A.)PbI$_3$(FAPbI$_3$) with 10 mol.% PbI$_2$, 10 mol.% MABr, and 40 mol.% MACl in *N,N*-dimethylformamide (DMF) and dimethylsulfoxide (DMSO) = (8:1 v/v) was prepared. And the precursor solution was coated onto the substrate at 1000 for 30 s and 5000 rpm at 10 s with dripping by diethyl ether. The coated films were annealed onto the hotplate at 150 °C for 10 min. To form a hole transporting layer, spiro-MeOTAD of 86 mg mL^{-1} in chlorobenzene solution with additives of 20 µL Li bis(trifluoromethanesulfonyl)imide (Li-TFSI)/acetonitrile (500 mg mL^{-1}), FK 209 Co(III) TFSI/acetonitrile (230 mg mL^{-1}) and 35 µL of 4-*tert*-butylpyridine (TBP) was spin-coated on the perovskite coated film at 3000 rpm for 30 s. Finally, the Au counter electrode has been deposited by thermal evaporation. A metal mask with an active area of 0.094 cm^2 was used to get reliable *J–V* curves.

Scheme 2. Comparison of Solar cell PCE and π phase change voltage of multi-functional devices. Data for multi-functional devices are adopted from various references.

Supporting Information

Supporting Information is available from the Wiley Online Library or from the author.

Acknowledgements

Conflict of Interest

The authors declare no conflict of interest.

Data Availability Statement

Research data are not shared.

Keywords

[1] M. Taguchi, A. Yano, S. Tohoda, K. Matsuyama, Y. Nakamura, T. Nishiwaki, K. Fujita, E. Maruyama, *IEEE J. Photovolt* **2014**, *4*, 96.
[2] S. Essig, S. Ward, M. A. Steiner, D. J. Friedman, J. F. Geisz, P. Stradins, D. L. Young, *Energy Procedia* **2015**, *77*, 464.
[3] M. H. Futscher, B. Ehrler, *ACS Energy Lett.* **2016**, *1*, 863.
[4] K. Yoshikawa, H. Kawasaki, W. Yoshida, T. Irie, K. Konishi, K. Nakano, T. Uto, D. Adachi, M. Kanematsu, H. Uzu, K. Yamamoto, *Nat. Energy* **2017**, *2*, 17032.
[5] M. A. Green, Y. Hishikawa, E. D. Dunlop, D. H. Levi, J. Hohl-Ebinger, M. Yoshita, A. W. Y. Ho-Baillie, *Prog. Photovolt: Res. Appl.* **2019**, *27*, 3.
[6] G. Fulop, M. Doty, P. Meyers, J. Betz, C. H. Liu, *Appl. Phys. Lett.* **1982**, *40*, 327.
[7] J. D. Poplawsky, *Nat. Energy* **2016**, *1*, 16021.
[8] D. Cunningham, M. Rubcich, D. Skinner, *Prog. Photovolt: Res. Appl.* **2002**, *10*, 159.
[9] M. A. Matin, M. Mannir Aliyu, A. H. Quadery, N. Amin, *Sol. Energy Mater. Sol. Cells* **2010**, *94*, 1496.
[10] H.-W. Schock, R. Noufi, *Prog. Photovolt: Res. Appl.* **2000**, *8*, 151.
[11] P. Jackson, D. Hariskos, R. Wuerz, O. Kiowski, A. Bauer, T. M. Friedlmeier, M. Powalla, *Phys. Status Solidi RRL* **2015**, *9*, 28.
[12] H. J. Snaith, *J. Phys. Chem. Lett.* **2013**, *4*, 3623.
[13] N. J. Jeon, J. H. Noh, Y. C. Kim, W. S. Yang, S. Ryu, S. I. Seok, *Nat. Mater.* **2014**, *13*, 897.
[14] H. Zhang, J. Mao, H. He, D. Zhang, H. L. Zhu, F. Xie, K. S. Wong, M. Grätzel, W. C. H. Choy, *Adv. Energy Mater.* **2015**, *5*, 1501354.
[15] A. Kojima, K. Teshima, Y. Shirai, T. Miyasaka, *J. Am. Chem. Soc.* **2009**, *131*, 6050.
[16] H. Min, D. Y. Lee, J. Kim, G. Kim, K. S. Lee, J. Kim, M. J. Paik, Y. K. Kim, K. S. Kim, M. G. Kim, T. J. Shin, S. Il Seok, *Nature* **2021**, *598*, 444.
[17] J.-H. Lee, J. Kim, T. Y. Kim, M. S. Al Hossain, S.-W. Kim, J. H. Kim, *J. Mater. Chem. A* **2016**, *4*, 7983.
[18] D. Tainoff, A. Proudhom, C. Tur, T. Crozes, S. Dufresnes, S. Dumont, D. Bourgault, O. Bourgeois, *Nano Energy* **2019**, *57*, 804.
[19] A. R. M. Khairudin, H. Salleh, *A.I.P. Conf. Proc* **2018**, *2030*, 020042.
[20] G. Gou, N. Charles, J. Shi, J. M. Rondinelli, *Inorg. Chem.* **2017**, *56*, 11854.
[21] S. Siddiqui, D.-I. Kim, L. T. Duy, M. T. Nguyen, S. Muhammad, W.-S. Yoon, N.-E. Lee, *Nano Energy* **2015**, *15*, 177.
[22] S. K. Karan, R. Bera, S. Paria, A. K. Das, S. Maiti, A. Maitra, B. B. Khatua, *Adv. Energy Mater.* **2016**, *6*, 1601016.
[23] X. Ren, H. Fan, Y. Zhao, Z. Liu, *A.C.S. Appl. Mater. Interfaces* **2016**, *8*, 26190.
[24] X. Chen, X. Li, J. Shao, N. An, H. Tian, C. Wang, T. Han, L. Wang, B. Lu, *Small* **2017**, *13*, 1604245.
[25] M. Coll, A. Gomez, E. Mas-Marza, O. Almora, G. Garcia-Belmonte, M. Campoy-Quiles, J. Bisquert, *J. Phys. Chem. Lett.* **2015**, *6*, 1408.
[26] H.-S. Kim, S. K. Kim, B. J. Kim, K.-S. Shin, M. K. Gupta, H. S. Jung, S.-W. Kim, N.-G. Park, *J. Phys. Chem. Lett.* **2015**, *6*, 1729.
[27] A. D. Schulz, H. Röhm, T. Leonhard, S. Wagner, M. J. Hoffmann, A. Colsmann, *Nat. Mater.* **2019**, *18*, 1050.
[28] Y. Bai, T. Siponkoski, J. Peräntie, H. Jantunen, J. Juuti, *Appl. Phys. Lett.* **2017**, *110*, 063903.
[29] F. Cao, H. Wang, P. Shen, X. Li, Y. Zheng, Y. Shang, J. Zhang, Z. Ning, X. Yang, *Adv. Funct. Mater.* **2017**, *27*, 1704278.
[30] Y.-J. Kim, T.-V. Dang, H.-J. Choi, B.-J. Park, J.-H. Eom, H.-A. Song, D. Seol, Y. Kim, S.-H. Shin, J. Nah, S.-G. Yoon, *J. Mater. Chem. A* **2016**, *4*, 756.
[31] Q. Lai, L. Zhu, Y. Pang, L. Xu, J. Chen, Z. Ren, J. Luo, L. Wang, L. Chen, K. Han, P. Lin, D. Li, S. Lin, B. Chen, C. Pan, Z. L. Wang, *ACS Nano* **2018**, *12*, 10501.
[32] Q. Dong, J. Song, Y. Fang, Y. Shao, S. Ducharme, J. Huang, *Adv. Mater.* **2016**, *28*, 2816.
[33] Y. Guo, C. Liu, H. Tanaka, E. Nakamura, *J. Phys. Chem. Lett.* **2015**, *6*, 535.
[34] K. T. Cho, G. Grancini, Y. Lee, E. Oveisi, J. Ryu, O. Almora, M. Tschumi, P. A. Schouwink, G. Seo, S. Heo, J. Park, J. Jang, S. Paek, G. Garcia-Belmonte, M. K. Nazeeruddin, *Energy Environ. Sci.* **2018**, *11*, 952.
[35] Q. Jiang, Y. Zhao, X. Zhang, X. Yang, Y. Chen, Z. Chu, Q. Ye, X. Li, Z. Yin, J. You, *Nat. Photonics* **2019**, *13*, 460.
[36] K. C. Mandal, S. K. Chaudhuri, K. V. Nguyen, M. A. Mannan, *IEEE Trans. Nucl. Sci.* **2014**, *61*, 2338.
[37] A. Rohatgi, R. H. Hopkins, J. R. Davis, R. B. Campbell, H. C. Mollenkopf, *Solid State Electron* **1980**, *23*, 1185.
[38] Q. Zhang, Q. Song, X. Wang, J. Sun, Q. Zhu, K. Dahal, X. Lin, F. Cao, J. Zhou, S. Chen, G. Chen, J. Mao, Z. Ren, *Energy Environ. Sci.* **2018**, *11*, 933.
[39] S. Heo, G. Seo, Y. Lee, D. Lee, M. Seol, J. Lee, J.-B. Park, K. Kim, D.-J. Yun, Y. S. Kim, J. K. Shin, T. K. Ahn, M. K. Nazeeruddin, *Energy Environ. Sci.* **2017**, *10*, 1128.
[40] S. Heo, G. Seo, K. T. Cho, Y. Lee, S. Paek, S. Kim, M. Seol, S. H. Kim, D.-J. Yun, K. Kim, J. Park, J. Lee, L. Lechner, T. Rodgers,

ADVANCED
SCIENCE NEWS

www.advancedsciencenews.com

ADVANCED
ENERGY
MATERIALS

www.advenergymat.de

J. W. Chung, J.-S. Kim, D. Lee, S.-H. Choi, M. K. Nazeeruddin, *Adv. Energy Mater.* **2019**, *9*, 1902470.

[41] S. Heo, G. Seo, Y. Lee, M. Seol, S. H. Kim, D.-J. Yun, Y. Kim, K. Kim, J. Lee, J. Lee, W. S. Jeon, J. K. Shin, J. Park, D. Lee, M. K. Nazeeruddin, *Adv. Mater.* **2019**, *31*, 1805438.

[42] W. Dong, D. Cortie, T. Lu, Q. Sun, N. Narayanan, W. Hu, L. Jacob, Q. Li, D. Yu, H. Chen, A. Chen, X. Wei, G. Wang, M. G. Humphrey, T. J. Frankcombe, Y. Liu, *Mater. Horiz.* **2019**, *6*, 1717.

[43] L. Li, X. Cheng, J. R. Jokisaari, P. Gao, J. Britson, C. Adamo, C. Heikes, D. G. Schlom, L.-Q. Chen, X. Pan, *Phys. Rev. Lett.* **2018**, *120*, 137602.

[44] S. Mandal, T. Skála, K. S. R. Menon, *J. Mater. Chem. C* **2021**, *9*, 595.

[45] M. D. Nguyen, T. Q. Trinh, M. Dekkers, E. P. Houwman, H. N. Vu, G. Rijnders, *Ceram. Int.* **2014**, *40*, 1013.

[46] J. M. Vail, D. Schindel, A. Yang, O. Penner, R. Pandey, H. Jiang, M. A. Blanco, A. Costales, Q. C. Qiu, Y. Xu, *J. Phys. Condens. Matter* **2004**, *16*, 3371.

[47] F. Li, M. J. Cabral, B. Xu, Z. Cheng, E. C. Dickey, J. M. LeBeau, J. Wang, J. Luo, S. Taylor, W. Hackenberger, L. Bellaiche, Z. Xu, L.-Q. Chen, T. R. Shrout, S. Zhang, *Science* **2019**, *364*, 264.

[48] F. Li, D. Lin, Z. Chen, Z. Cheng, J. Wang, C. Li, Z. Xu, Q. Huang, X. Liao, L.-Q. Chen, T. R. Shrout, S. Zhang, *Nat. Mater.* **2018**, *17*, 349.

[49] E. Jia, D. Wei, P. Cui, J. Ji, H. Huang, H. Jiang, S. Dou, M. Li, C. Zhou, W. Wang, *Adv. Sci.* **2019**, *6*, 1900252.

[50] B. Chen, X. Zheng, M. Yang, Y. Zhou, S. Kundu, J. Shi, K. Zhu, S. Priya, *Nano Energy* **2015**, *13*, 582.

[51] B. Chen, J. Shi, X. Zheng, Y. Zhou, K. Zhu, S. Priya, *J. Mater. Chem. A* **2015**, *3*, 7699.